Journal of Applied Electrochemistry **33**: 823–830, 2003.
© 2003 *Kluwer Academic Publishers. Printed in the Netherlands.*

Void-free anisotropic deposition for IC interconnect with polyethylene glycol as the single additive based on uneven adsorption distribution

B.-H. WU, C.-C. WAN* and Y.-Y. WANG
Department of Chemical Engineering, Tsing-hua University, Hsin-Chu, Taiwan 300
*(*author for correspondence, fax: +886 3 5715408; e-mail: ccwan@mx.nthu.edu.tw)*

Received 4 February 2003; accepted in revised form 2 April 2003

Key words: adsorption, adsorption isotherm, copper interconnection, current–potential hysteresis, polyethylene glycol, superfilling

Abstract

The adsorption behaviour of polyethylene glycol (PEG) in the presence of chloride ion in an acid copper electrolyte was investigated by several electrochemical methods including chronopotentiometry, linear sweep voltammetry, cyclic voltammetry and electrochemical impedance. Surface coverages calculated from the chronopotentiometry measurement were fitted into the Toth isotherm with good agreement. The standard free energy of PEG adsorption, ΔG°_{ads}, evaluated to be −51.67 kJ mol^{-1} indicates strong interaction between PEG and the copper surface. Current–potential hysteresis was found in bath with low PEG concentration as the result of low PEG adsorption rate. Void-free anisotropic deposition for IC copper interconnect can thus be achieved with the addition of PEG only by properly adjusting its concentration based on its adsorption behaviour.

List of symbols

i_{add}	current density in additive contained bath (A dm^{-2})
i_{no}	current density in no additive contained bath (A dm^{-2})
C_{Cu}	concentration of $CuSO_4$ at electrode surface (M)
$C_{H_2SO_4}$	concentration of H_2SO_4 at electrode surface (M)
F	faradaic constant (96 487 C mol^{-1})
R	universal gas constant (8.314 J mol^{-1} K^{-1})
T	absolute temperature (K)
n	number of electrons transferred in deposition
C^{b}_{Cu}	bulk concentration of $CuSO_4$ (M)
$C_{dl,0}$	double layer capacitance in deposition bath without additive (μF cm^{-2})
C_{dl}	double layer capacitance in deposition bath with additive (μF cm^{-2})
$C_{dl,ML}$	double layer capacitance with a monolayer additive (μF cm^{-2})
K_{equ}	equilibrium constant of adsorption (L mol^{-1})
ΔG°_{ads}	standard free energy of adsorption (J mol^{-1})

Greek symbols

θ	surface coverage
η	activation overpotential (V)
ϕ_A	applied potential (V)
ϕ_e	equilibrium cell potential (V)
η_{IR}	ohmic overpotential (V)
η_c	concentration overpotential (V)
$\theta_{\Delta V}$	surface coverage obtained by chronopotentiometry
$\phi_{A,no}$	applied potential in deposition bath without additive (V)
$\theta_{C_{dl}}$	surface coverage obtained by EIS
α_{To}, c_{To}	parameters in Toth isotherm

1. Introduction

The damascene process for fabrication of copper interconnects requires void-free deposition into submicron trenches or vias. Since these trenches and vias are always of high aspect ratio, void-free (or, superfilling) deposition can be realized only when the deposition rate is higher in the bottom of the via than at the entrance. Previous experiments show that suitable choice of a multicomponent additive package can achieve void-free deposition [1, 2]. The additives are usually composed of polyethylene glycol (PEG), bis(3-sulfopropyl) disulfide (SPS) and Janus Green B (JGB) [1] or PEG and 3-mercapto-1-propanesulfonate (MPSA) [2], which can all result in superfilling deposition. Among those additives, PEG functions as the suppressor because of its strong inhibition on reaction kinetics, especially when chloride ion is present [3–6]. SPS and MPSA, generally called the accelerator, speed up the deposition rate [1, 2]. A theoretical model has been developed to show the competitive adsorption of these additives on the electrode surface which results in various current density distributions and with some particular additive compositions,

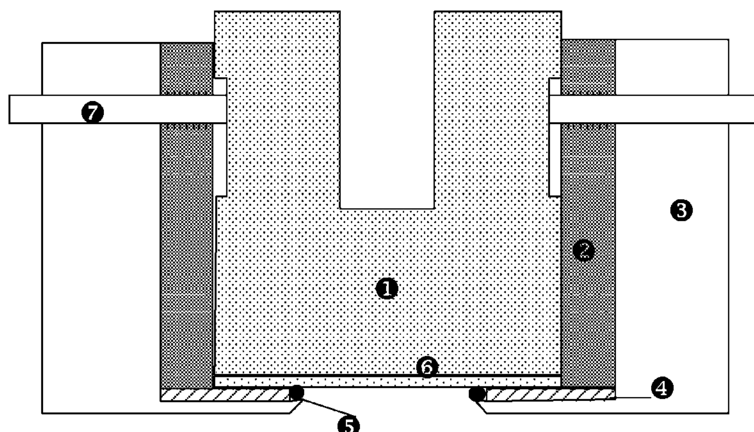

Fig. 1. RDE adaptor for wafer fragment deposition. Legend: (1): copper, (2) aluminium, (3) teflon, (4) copper flake, (5) O-ring, (6) wafer fragment and (7) screw.

void-free deposition occurs [7, 8]. Analysis of the current–potential hysteresis can illustrate the competitive adsorption of additives [9].

Most previous articles on void-free deposition focus on the behaviour of accelerators (SPS and MPSA) because, in practice, a particular phenomenon called overfill can not be well explained by the traditional diffusion–adsorption mechanism of the additives [10]. The results from previous work also show that superfilling is only achievable if the additives are in a threecomponent (suppressor, leveller and accelerator) or two-component (suppressor and accelerator) arrangement [1, 2, 11]. The only exception is a paper recently published by Hayase et al., which shows the consumption of the chloride ion at the via bottom can break down the PEG-Cl inhibition, resulting in superfilling with only one-component additive [12]. However, detailed study pertaining to PEG adsorption behaviour to superfilling deposition is still insufficient. In this study, we have employed several electrochemical methods such as chronopotentiometry, linear sweep voltammetry (LSV), cyclic voltammetry (CV) and electrochemical impedance (EIS) to conduct a detailed study on PEG adsorption. Information obtained may help us to improve additive formulation for superfilling in via with size around 0.18 μm and aspect ratio about 2–4.

2. Experimental details

A fragment of wafer was firstly mounted in the rotating disc electrode (RDE) adaptor, as shown in Figure 1. The design of the adaptor basically follows that reported by Taephaisitphongse et al. [1]. Before deposition, the electrical contact resistance of the system was checked to make sure it was negligible. Three different electrolytes were used in this study, including predeposition, deposition and stripping baths. The predeposition and stripping baths were used for CV measurements after the filling experiments. The deposition bath was composed of 0.2 M $CuSO_4$, 1 M H_2SO_4, 2.174 mM (180 μL L^{-1}) HCl plus PEG (MW $\approx$ 3200) in various concentrations. All were of analytical grade. The RDE was then immersed into the bath and deposition proceeded for 120 s.

As for CV experiments, a platinum RDE (dia. 4.5 mm) was initially deposited with copper with 1 mA current for 180 s in the predeposition bath, which contained 0.2 M $CuSO_4$ and 1 M H_2SO_4. Three cycles of CV, with scan rate at 50 mV s^{-1} and potentials between −0.2 and 0.1 V with respect to the open circuit potential (OCP), were subsequently applied to obtain a reproducible surface state. The electrode was then transferred into deposition bath for two CV experiments of different scan rates (100 and 10 mV s^{-1}). As CV scanning finished, the electrode was transferred into the stripping bath to strip off the copper and, it was then immersed in piranha agent ($H_2O_2/H_2SO_4 = 1{:}3$ in volume) to chemically remove the residual copper.

Other experiments also required predeposition and stripping steps as mentioned above. For experiments by electrochemical impendence spectroscopy, the electrode was polarized at −0.55 V with respect to SSE for 80 s to reach steady state before starting the EIS measurement. The impedence was measured at −0.55 V between 50 kHz and 0.05 Hz and the sine wave amplitude was controlled at 5 mV. The conditions for chronopotentiometry and LSV were 1ASD (1 A dm^{-2}) and 0 V to −0.4 V (with respect to OCP) with 0.5 mV s^{-1} scan rate, respectively. The cell was connected to a Schlumberger 1286 potentiostat for LSV, CV and chronopotentiometry measurements. EIS was performed using an Autolab (ECO Chemie, Holland) potentiostat coupled with a frequency response analyser.

3. Results and discussion

Several LSV experiments with electrolyte of various compositions to study the effect of chloride ion and PEG on the reaction kinetics were carried out. As shown in

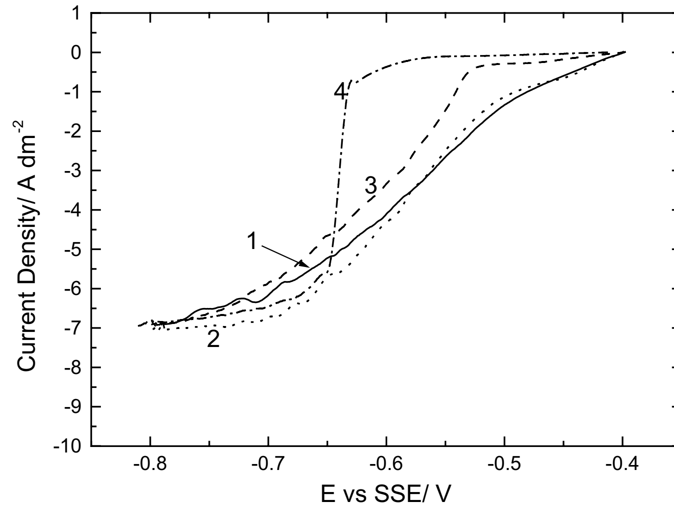

Fig. 2. LSV curves. Rotation speed of RDE is 100 rpm and potential scanning rate is 0.5 mV s^{-1}. Electrolyte composition: (1) base, $CuSO_4 \equiv 0.2$ M, $H_2SO_4 \equiv 1$ M; (2) base + 2.174 mM HCl; (3) base + 10^{-7} PEG; (4) base + 2.174 mM HCl + 10^{-7} M PEG.

Figure 2, at the same potential, the cathodic current of the base electrolyte (curve 1) is smaller than that in the presence of chloride ion (curve 2). This may be owing to the adsorption of ionic additives which changes the Helmholtz potential of the double layer (i.e., ϕ_2 effect) [13,14] or the chloride ion catalyses the reaction rate of Cu^{2+}/Cu^{+} step, which changes the reaction mechanism to an anionbridge, inner-sphere reaction [15]. The addition of PEG blocks the reaction sites and suppresses the reaction rate, so the current (curve 3) is lower than those without PEG (curve 1). As chloride ion is added into electrolyte in the presence of PEG, even more significant blocking effect occurs in the lower polarized region, that is, more positive than −0.65 V. The possible reason is the formation of PEG complexes ($[Cu^{+}\text{–}(CH_2\text{–})_3H_2O]$ or $[Cu^{2+}\text{–}(CH_2^{-})_4(H_2O)_2]$), rendering a loss of electroneutrality from the polymer molecules, which in turn results in the strong linkage between polymer complexes and the chloride ion adsorbing on the electrode surface [5, 16]. This strong blocking effect totally negates the catalytic behaviour of the chloride ion. Because the chloride ion and PEG change the deposition rate significantly, there is a possibility to apply this characteristic to accomplish void-free anisotropic deposition by precise control of the PEG adsorption.

Previous researchers have hypothesized that the current produced from a bath with additives is proportional to the fraction of the vacant sites on the electrode [17, 18],

$$i_{add} = i_{no}(1-\theta) \tag{1}$$

where θ is the surface coverage of the additive and i_{no} is the current without additive at the same activation overpotential. Substituting Equation 1 into the kinetic equation for acid copper deposition derived by Chapman et al. [19], we obtain

$$i_{add} = 15.6\, C_{Cu}^{0.67} e^{-0.37 C_{H_2SO_4}} \times \left\{ \exp\left(\frac{1.08\,\eta F}{RT}\right) - \exp\left(\frac{-0.39\,\eta F}{RT}\right) \right\} (1-\theta) \tag{2}$$

where i_{add} is the current density (mA cm^{-2}), η is the activation overpotential and C_{Cu}, $C_{H_2SO_4}$ are surface concentrations of copper ion and sulfuric acid, respectively. In practice, the deposition is under galvanostatic control, say 1 A dm^{-2}, so we are interested in the adsorption behaviour of PEG under this condition. The activation overpotential is a component of the overpotential as expressed in Equation (3),

$$\eta = \phi_A - \phi_e - \eta_{IR} - \eta_c \tag{3}$$

where ϕ_A, ϕ_e, η_{IR} and η_c represent the applied cell potential, equilibrium cell potential, ohmic overpotential and concentration overpotential, respectively. ϕ_e is approximately nil in this case and η_{IR} is also negligible when the conductivity of the electrolyte is fairly high. Substituting the approximate form of concentration overpotential shown in Equation 4, into Equations 2 and 3, the kinetic equation is rearranged as follows:

$$\eta_c = \frac{RT}{nF} \ln \frac{C_{Cu}}{C_{Cu}^{b}} \tag{4}$$

$$i_{add} = -15.6\, C_{Cu}^{0.67} e^{-0.37 C_{H_2SO_4}} \left\{ \exp\left(\frac{-0.39\,\phi_A F}{RT}\right) \right\} \times \left(\frac{C_{Cu}}{C_{Cu}^{b}}\right)^{0.195} (1-\theta) \tag{5}$$

where i_{add} is in mA cm^{-2}.

A similar expression can also be derived for the current (i_{no}) without the additive blocking effect. In the case of galvanostatic deposition, we may assume the

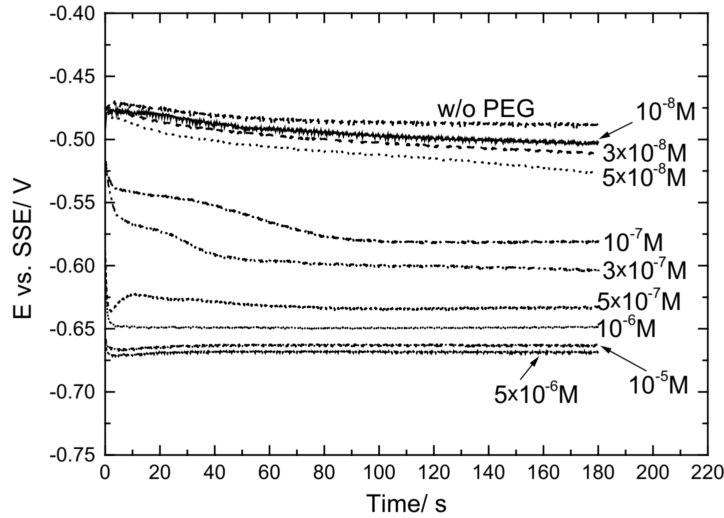

Fig. 3. Chronopotentiometry of the different PEG concentrations in 1 A dm^{-2}.

surface concentration of copper is the same with or without additive, so the expression for surface coverage, θ, may be derived as

$$\theta_{\Delta V} = 1 - \exp\left\{ -\frac{0.39F}{RT}\left(\phi_{\mathrm{A,no}} - \phi_{\mathrm{A}}\right) \right\} \tag{6}$$

where $\phi_{\mathrm{A,no}}$ is the applied cell potential in the case without additive and $\theta_{\Delta V}$ refers to the surface coverage measured by chronopotentiometry. Equation 6 can be used to calculate the surface coverage of PEG. Figure 3 shows the result by chronopotentiometry in different concentrations of PEG with the RDE controlled at 100 rpm. Assuming steady state can be established at the end of the deposition (i.e., after 180 s), the steady state potential for deposition becomes more negative as PEG concentration increases, because of the blocking effect of PEG adsorption. When the PEG concentration is between 10^{-7} M and 3×10^{-7} M, the electrode needs about 90 to 40 s before it reaches the steady state potential. It was reported that the adsorption rate is proportional to the adsorbate concentration [20], so the length of potential decay before reaching steady state may be directly related to the time needed to reach adsorption equilibrium. This interpretation implies that adsorption equilibrium may yet to be established after 180 s in cases with very low PEG concentration ($<5 \times 10^{-8}$ M). However, if we extend the deposition period, another problem may arise since the change of the electrode surface area could be significant with prolonged deposition. Thus, we assume that the steady state potential can be reached in 180 s in all cases. Figure 3 also shows the steady state potential approaches a limiting value as the PEG concentration is continuously increased, which indicates the blocking effect of PEG is becoming saturate.

Figure 4(a) and (b) depict the results of EIS for PEG of different concentrations. The double layer capacity, C_{dl}, derived from the EIS data is shown in Figure 4(c).

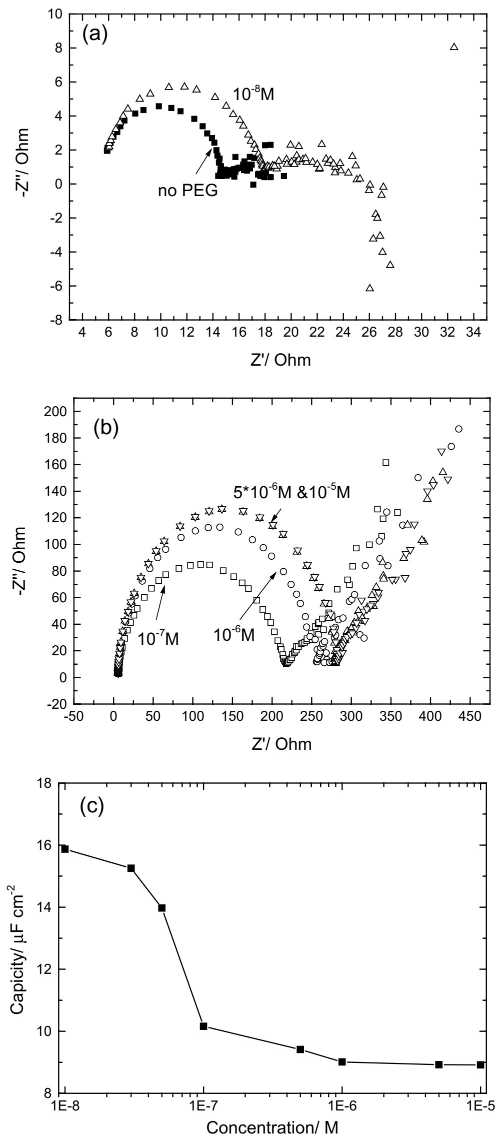

Fig. 4. (a) and (b) are EIS measurements for various PEG concentrations; (c) is the double layer capacity, which varies with respect to PEG concentration fitted by suitable equivalent circuit.

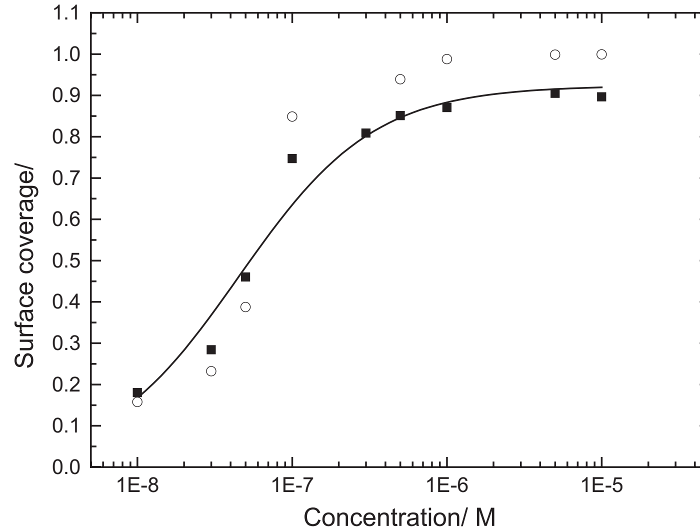

Fig. 5. Calculated surface coverage, $\theta_{\Delta V}$ and $\theta_{C_{dl}}$, as a function of PEG concentration. Toth model: $R^2 = 0.97$, $\alpha_{To} = 0.924$, $C_{To} = 0.995$, $K = 2.037 \times 10^7$ L mol^{-1}. Key: (■) Gal exp.; (○) E1S exp.; (—) Toth isotherm fitted with Gal exp.

Impedance data was fitted using a simple equivalent circuit, consisting of a resistor and a Warburg element in series, placed in parallel with a capacitor and then combined with an electrolyte resistance in series. Figure 4(a) shows the impedance data of electrolyte containing 0 M and 10^{-8} M PEG, respectively. The semicircles in Figure 4(a) are smaller than those in Figure 4(b), which may imply the adsorption of PEG increases the charge transfer resistance, especially in high PEG concentration. The diameter of the semicircle approaches a limiting value, as the PEG concentration is over 5×10^{-6} M. The capacity shown in Figure 4(c) decreases with increasing PEG concentration, which is expected since the adsorption of polymer is associated with the combined effects of a lower dielectric constant and an increase in thickness of the capacitor [21]. Because the electrolyte used is concentrated, we can neglect the diffuse double layer and focus on that part of the Helmholtz double layer which considers the electrode surface as a parallel-plate capacitor. So Frumkin's parallel-plate model can be applied to estimate the surface coverage of PEG from EIS data [14, 21, 22]. If we neglect the potential dependence of θ in Frumkin's model, the expression becomes

$$\theta_{C_{dl}} = \frac{C_{dl,0} - C_{dl}}{C_{dl,0} - C_{dl,ML}} \tag{7}$$

where $C_{dl,0}$ and $C_{dl,ML}$ are the capacitances without PEG adsorption and with a monolayer coverage of PEG, respectively.

Figure 5 shows the surface coverage calculated by Equations 6 and 7. Apparently, the increase of PEG concentration from 10^{-8} to 10^{-7} M enhances the surface coverage from 0.2 to 0.75. Further addition of PEG leads to a saturate surface coverage at about 0.91. The change of $\theta_{C_{dl}}$ also shows the same tendency as $\theta_{\Delta V}$. However, the maximum $\theta_{C_{dl}}$ approaches 1, which is larger than $\theta_{\Delta V}$ at the same PEG concentration. One possible reason is the inherent difference between galvanostatic and potentiostatic measurements (i.e., the current density is not 1 A dm^{-2} in EIS), so that the measured surface coverage will be different responding to different current densities. The other reason may be the choice of $C_{dl,ML}$ value, which in this study is assumed equal to the capacitance of saturated adsorption calculated in 10^{-5} M PEG. The assumption is not rigorously true because the capacitance of saturated adsorption may not be the same as that of the monolayer coverage. Moreover, the influence of the electrode surface roughness on the measurement of double layer capacity could also contribute to this discrepancy [27, 28]. However, the EIS measurements are still meaningful because the similar tendency between $\theta_{C_{dl}}$ and $\theta_{\Delta V}$ demonstrates the applicability of Equation 6.

The $\theta_{\Delta V}$ data for deposition at 1 A dm^{-2} were further fitted with the Toth isotherm and good agreement was found. The Toth isotherm, as shown in Equation 8, is a modification of the Langmuir isotherm by introducing two extra parameters, α_{To} and c_{To} [20, 23]:

$$\theta^{c_{To}} = \frac{\alpha_{To} C^{c_{To}}}{\frac{1}{K_{equ}} + C^{c_{To}}} \tag{8}$$

The fitting results are shown in Figure 5. The value of α_{To} and c_{To}, all close to 1, implies that the PEG adsorption isotherm does not deviate much from Langmuir isotherm. A fairly large equilibrium constant for adsorption, K_{equ}, indicates that the adsorption rate constant is much larger than the desorption rate constant. The standard free energy of adsorption ΔG°_{ads} is related to K_{equ} by the following equation:

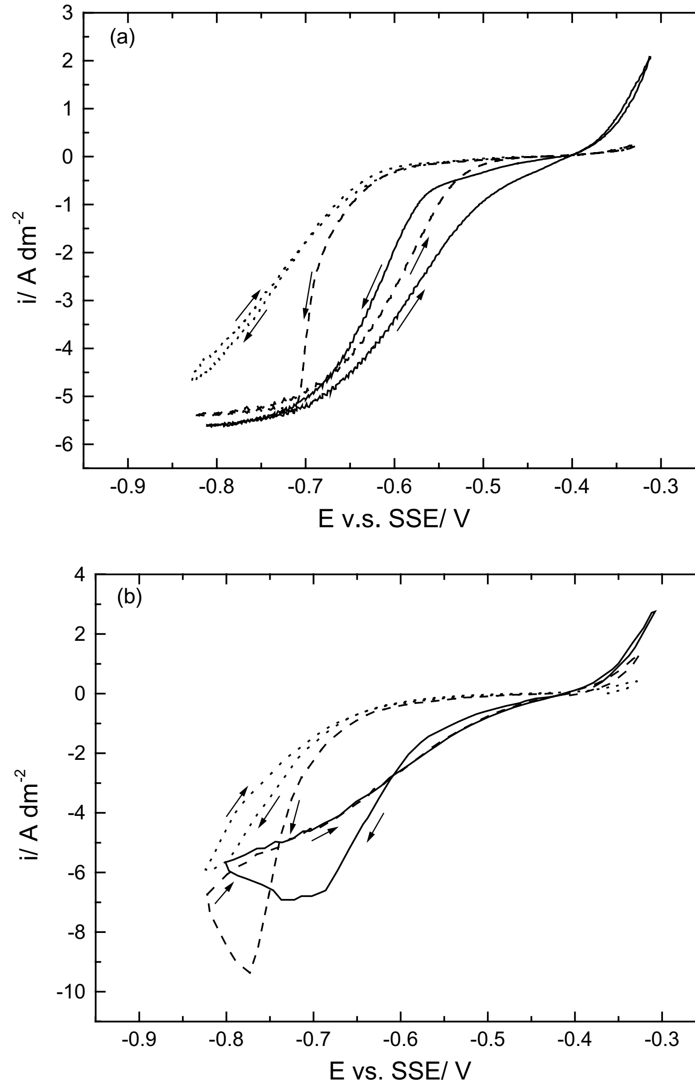

Fig. 6. CV of different PEG concentrations in low (10 mV s^{-1}) and high (100 mV s^{-1}) scan rates. Hysteresis is found in low PEG concentration. RDE rotation speed 100 rpm. Key: (—) 10^{-7} M, (- - - -) 10^{-6} M and (···) 10^{-5} M.

$$K_{equ} = \frac{1}{55.5} \exp\left(\frac{-\Delta G^{\circ}_{ads}}{RT}\right) \tag{9}$$

where 55.5 is the concentration of water in the solution in mol L^{-1}. The value of standard free energy for PEG adsorption ΔG°_{ads} is -51.67 kJ mol^{-1}, which is of the same order of magnitude as previously reported for adsorption of coumarin on nickel [22] and the adsorption of organic corrosion inhibitor on iron and gold [24]. The large negative value of ΔG°_{ads} indicates strong adsorption of PEG on copper surface.

Previous literature indicates that competitive adsorption between suppressor (PEG) and accelerator (SPS or MPSA) results in a current-potential hysteresis in CV data [2, 7, 9, 10]. This characteristic plays an important role in void free deposition and is essential in the mechanism of superfilling deposition. However, we have surprisingly found that the hysteresis also occurs even when only PEG is added to the electrolyte. Figures 6(a) and (b) are the CV diagrams with RDE rotation speed of 100 rpm. Three PEG concentrations were measured with scan rates at 10 and 100 mV s^{-1}, respectively. For low-scanning rate CV, typical current–potential hysteresis occurs between 10^{-7} and 10^{-6} M PEG, as shown in Figure 6(a). Since there is no accelerator in the electrolyte, the competitive adsorption mechanism for CV hysteresis is not applicable in our case. The other possible mechanism, PEG incorporation model, also deduced by Hebert for analysing CV hysteresis, leads to the predicted mole fraction of PEG in deposit being much higher than the organic impurity mole fractions actually measured [9], which may imply that the carbon content calculated by the PEG incorporation model needs modification. Thus, the hysteresis curves shown in Figure 6(a) cannot be adequately explained in terms of mechanisms previously developed.

According to the potential decays shown in Figure 3 and the calculation result of surface coverage shown in Figure 5, we know that PEG adsorption takes a period

of time and the surface coverage of 10^{-7} and 10^{-6} M PEG are not saturated. So, those PEG molecules having desorbed in the forward scan cannot immediately return to the electrode surface as the reverse scan begins. The low adsorption rate for low concentration PEG may be the reason for the hysteresis behaviour shown in Figure 6(a), since PEG concentrations in previous studies were all above 10^{-5} m [1–4, 7–10, 12]. Figure 6(a), in fact, also shows there is no hysteresis in the 10^{-5} M PEG case. The latter case may be the result of oversaturation of the surface coverage (according to Figure 5) and the fast adsorption rate of PEG in this relatively high concentration case.

Figure 6(b) shows the CV responses at high scan rate (100 mV s^{-1}). For PEG concentrations of 10^{-7} and 10^{-6} M, peak currents (7 and 9.4 A dm^{-2}) appear instead of the limiting current shown in Figure 6(a). This is because the scan rate (100 mV s^{-1} in this case) is relatively high and thus the rate of hydrodynamic supply of copper ion is lower than the deposition flux on the electrode surface. So, the diffusion boundary layer thickens and the peak current appears. The reverse scans of 10^{-7} and 10^{-6} M PEG intersects with their corresponding forward scans as the result of PEG desorption, rendering the current higher than that at the same potential in the forward scan. The current responses for the reverse scan in 10^{-7} and 10^{-6} M PEG almost overlap each other, which provides additional evidence to that mentioned above, namely, the adsorption rate for PEG returning to the electrode surface is slow in the reverse scan period for low PEG concentration, which results in insufficient suppressor on the surface and consequently a larger current in the reverse scan than in the forward scan, which, in turn, causes the formation of hysteresis in this one-component additive system. The potential at which the current increases abruptly in PEG = 10^{-7} M case is more positive than that in Figure 2, maybe as a result of Cl^{-} or PEG consumption, because the CV experiments were measured after filling experiments, while in Figure 2, fresh electrolyte was used. The peak potential in the 10^{-6} M case is more negative than that in the 10^{-7} M case, which implies that the increase in PEG concentration increases the charge transfer resistance. This is to be expected since the basic function of PEG is to act as a suppressor.

Since the surface coverage of 10^{-7} and 10^{-6} M PEG are not over saturated and show hysteresis in the CV diagram, the question arises as to whether void-free deposition can be accomplished based on this characteristic. Figure 7(A)–(C) are the SEM photographs for deposition in systems containing 10^{-7}, 10^{-6} and 10^{-5} M PEG, respectively. The white marks are protruding lines due to sectioning. It is obvious that void free deposition only occurs in the PEG = 10^{-6} M case, in contrast to results in 10^{-7} M and 10^{-5} M cases. The results can be explained by the adsorption isotherm in Figure 5. Because the deposition conditions are the same in both adsorption and filling experiments (i.e., 100 rpm and 1 A dm^{-2}), the surface coverage of PEG obtained from

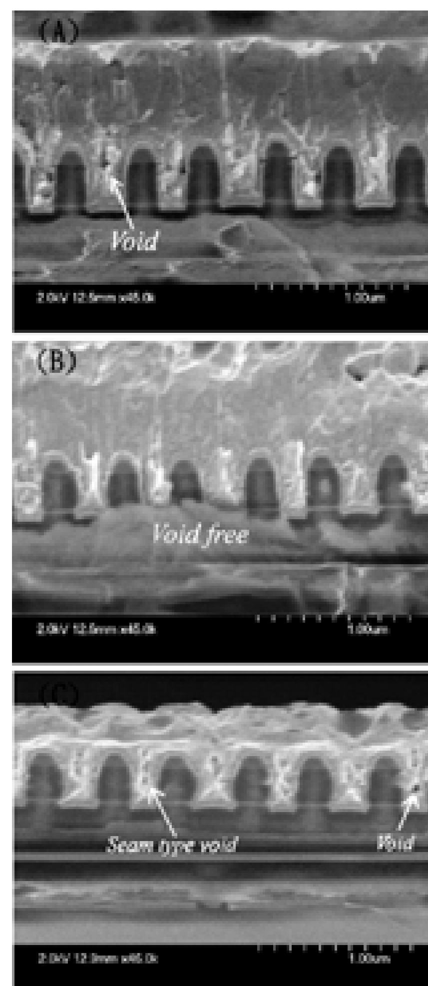

Fig. 7. SEM photographs for filling experiments in different PEG concentrations. (A)–(C) are 10^{-7} M, 10^{-6} M and 10^{-5} M, respectively.

the flat electrode surface in the adsorption experiment can be regarded as the surface coverage at the via opening of the pattern wafer. In the 10^{-5} M case, the surface coverage of PEG is oversaturated, so there is a possibility that not only the entrance but also the bottom of vias may all be fully inhibited, which results in conformal deposition. Thus, we can see the voids in Figure 7(C) are almost in seam types.

Voids in the 10^{-7} M PEG case can be attributed to insufficient inhibition at the via entrances, because the surface coverage according to Figure 5 is only about 0.7 at that location. The surface coverage at the entrance is insufficient, hence the inhibition effect at the entrance is not enough to induce a nonuniform deposition distribution along the via wall. The surface coverage of PEG in the 10^{-6} M case meets the saturation condition so there is a possibility that the surface coverage inside the vias is not saturated because of the geometrical hindrance for PEG mass transfer. The difference between saturated and nonsaturated PEG adsorption at the opening and inside the vias causes corresponding different deposition rates, whereby a void free deposition in the PEG = 10^{-6} M case is obtained. Accordingly, void-free anisotropic deposition can be accomplished

Table 1. Comparison of the bath compositions and filling mechanisms in previous work and this study

	$CuSO_4/H_2SO_4$	Cl^-	Suppressor PEG	Accelerator	Leveller	Filling mechanism
West [1]	0.24 M/1.8 M	50 ppm	8.82×10^{-5} M	SPS 1–2 ppm	JGB 2 ppm	Competitive adsorption
Moffat [2]	0.25 M/1.8 M	10^{-3} M	8.82×10^{-5} M	MPSA 10^{-5} M	w/o	Competitive adsorption
Hayase [12]	0.9 M/0.56 M	2×10^{-4} M	10^{-4} M	w/o	w/o	Breakdown PEG-Cl inhibition
This work	0.2 M/1 M	2.17×10^{-3} M	10^{-6} M	w/o	w/o	Uneven adsorption distribution

simply by adjusting the PEG concentration based on its adsorption behaviour and no accelerator is needed.

Table 1 is a summary of bath compositions and filling mechanisms regarding superfilling of IC vias. The bath compositions in the work of West [1] and Moffat [2] are basically the same, except for the choice of accelerator and leveller. The filling mechanisms in both cases are all based on the competitive adsorption of accelerator to leveller or suppressor. According to Hayase [12], higher $CuSO_4$ concentration and lower H_2SO_4 concentration are used because theoretical models show that a lower concentration gradient of copper inside the via benefits the filling ability [25, 26]. The chloride concentration is the lowest, so that it will be comparably easier to breakdown PEG-Cl inhibition inside the via, which is essential since there is no accelerator in this bath. In our bath, the choice of base electrolyte composition follows the theoretical calculation in our previous study [25]. The basic composition is similar to that of West [1] and Moffat [2]; however, the chloride ion concentration is the highest among the four systems, which ensures that the breakdown of PEG-Cl inhibition is unlikely in our case. The concentration of PEG in this work is about two orders lower than that in the others, so that PEG adsorption is not saturated inside the via, which results in void-free deposition.

4. Conclusions

The kinetics of copper deposition in electrolytes containing Cl^-, PEG and $Cl^- +$ PEG show large deviations from each other. These complex phenomena render the idea of accomplishing void-free anisotropic deposition by using a single-component PEG additive very attractive. The surface coverage of PEG can be calculated from data by either chronopotentiometry or by EIS measurements. The Toth isotherm fits the experimental results quite well and the large adsorption equilibrium constant evaluated implies that the interaction between PEG and the copper surface is strong. The surface coverage of PEG increases from 0.2 to 0.75 as the PEG concentration is increased from 10^{-8} to 10^{-7} M and it shows a saturated value when the concentration is higher than 5×10^{-6} M. Current-potential hysteresis is found in the case of low PEG concentration. The hysteresis curve is the result of the low adsorption rate of PEG in the low concentration cases. The adsorption of PEG in the low concentration range can be exploited to design a nonuniform adsorption of PEG from the entrance to the bottom of the vias, which can lead to void-free deposition of copper for IC interconnect without the need for accelerator.

Acknowledgement

The work was supported by the National Science Council (Project 90-2214-E-007-007) and the Chang Chun Petrochemical Co.

References

1. P. Taephaisitphongse, Y. Cao and A.C. West, *J. Electrochem. Soc.* **148** (2001) C492.
2. T.P. Moffat, J.E. Bonevich, W.H. Huber, A. Stanishevsky, D.R. Kelly, G.R. Stafford and D. Josell, *J. Electrochem. Soc.* **147** (2000) 4524.
3. J.J. Kelly and A.C. West, *J. Electrochem. Soc.* **145** (1998) 3472.
4. J.J. Kelly and A.C. West, *J. Electrochem. Soc.* **145** (1998) 3477.
5. D. Stoychev, *Trans IMF* **76**(2) (1998) 73.
6. J.D. Reid and A.P. David, *Plat. Surf. Finish.* **74** (1987) 66.
7. T.P. Moffat, D. Wheeler, W.H. Huber and D. Josell, *Electrochem.* & Solid-State Lett. **4**(4) (2001) C26.
8. Y. Cao, P. Taephaisitphongse and A.C. West, *J. Electrochem. Soc.* **148** (2001) C466.
9. K.R. Hebert, *J. Electrochem. Soc.* **148** (2001) C726.
10. A.C. West, S. Mayer and J. Reid, *Electrochem.* & Solid-State Lett. **4** (2001) C50.
11. W.C. Gau and T.C. Chang, *J. Vac. Sci. Technol. A* **18** (2000) 656.
12. M. Hayase, M. Taketani, K. Aizawa, T. Hatsuzawa and K. Hayabusa, *Electrochem.* & *Solid-State Lett.* **5**(10) (2002) C98.
13. T.C. Franklin, *Plat. Surf. Finish.* **81** (1994) 62.
14. A.J. Bard and L.R. Faulkner, 'Electrochemical Methods' (J. Wiley & Sons, New York, 2nd edn, 2001), and references therein.
15. Z. Nagy, J.P. Blaudeau, N.C. Hung, L.A. Curtiss and D.J. Zurawski, *J. Electrochem. Soc.* **142** (1995) L87.
16. D. Stoychev and C. Tsvetanov, *J. Appl. Electrochem.* **26** (1996) 741.
17. K.G. Jordan and C.W. Tobias, *J. Electrochem. Soc.* **138** (1991) 1251.
18. C. Madore and D. Landolt, *J. Electrochem. Soc.* **143** (1996) 3936.
19. R. Cabán and T.W. Chapman, *J. Electrochem. Soc.* **124** (1977) 1371.
20. R.I. Masel, 'Principles of Adsorption and Reaction on Solid Surfaces' (J. Wiley & Sons, New York, 1996), and references therein.
21. E. Gileadi, 'Electrode Kinetics', (VCH, Weinheim, 1993), and references therein.
22. P. Kern and D. Landolt, *J. Electrochem. Soc.* **148** (2001) B228.
23. J. Toth, *Acta Chim. Acad. Sci. Hung.* **69** (1971) 311.
24. T. Mimani and S.M. Mayanna, *J. Electrochem. Soc.* **140** (1993) 984.
25. B.H. Wu, C.C. Wan and Y.Y. Wang, *J. Electrochem. Soc.* **150** (2003) C7.
26. A.C. West, C.C. Cheng and B.C. Baker, *J. Electrochem. Soc.* **145** (1998) 3070.
27. E. Lust, A. Janes, K. Lust, V. Sammelselg and P. Miidla, *Electrochim. Acta* **42** (1997) 2861.
28. G. Jarzabek and Z. Borkowska, *Electrochim. Acta* **42** (1997) 2915.